Supercontinuum generation from 2 to 20 μm in GaAs pumped by picosecond CO_2 laser pulses

J. J. Pigeon,* S. Ya. Tochitsky, C. Gong, and C. Joshi

Department of Electrical Engineering, University of California at Los Angeles, 405 Hilgard Avenue, Los Angeles, California 90095, USA
**Corresponding author: jpigeon@ucla.edu*

Received April 1, 2014; revised April 24, 2014; accepted April 25, 2014;
posted April 25, 2014 (Doc. ID 209361); published May 26, 2014

We report on the generation of supercontinuum radiation from 2 to 20 μm in a 67 mm long GaAs crystal pumped by a train of 3 ps CO_2 laser pulses. Temporal measurements indicate that sub-picosecond pulse splitting is involved in the production of such wide-bandwidth radiation in GaAs. The results show that the observed spectral broadening is heavily influenced by four-wave mixing and stimulated Raman scattering.

OCIS codes: (140.3470) Lasers, carbon dioxide; (190.0190) Nonlinear optics; (320.6629) Supercontinuum generation.
http://dx.doi.org/10.1364/OL.39.003246

Supercontinuum (SC) generation in a nonlinear medium is a common technique used to produce ultra-broadband visible and IR light for applications in optical-coherence tomography, broadband spectroscopy, and LIDAR measurements in the atmosphere [1]. The generation of SC spectra with greater than one octave of bandwidth has been demonstrated using femtosecond [2–6], picosecond [7], and nanosecond [8] laser pulses interacting with fibers that exhibit negative group velocity dispersion (GVD) at the pump wavelength. Here several nonlinear optical effects, such as self-phase modulation (SPM), stimulated Raman scattering (SRS), four-wave mixing (FWM), modulational instability (MI) for picosecond pulses, and soliton fission (SF) for femtosecond pulses play an important role in the generation of broadband light [9]. All of the above experiments in fibers use near-IR pump lasers (0.8–2 μm), thus limiting the generated frequencies in the mid-IR part of the spectrum. At present the broadest mid-IR SC sources covering the range from 0.8 to 5 μm are realized using IR fibers [4–6,8].

Many applications would benefit from a source covering the entire "molecular fingerprint region" from 2 to 20 μm. There are several materials, such as GaAs, CdTe, and InSb, which possess nonlinear coefficients $n_2 > (10^{-13}$ cm^2/W) and are highly transparent throughout the mid-IR spectral range. However, the optimal pump for SC generation in these crystals lies in the 7–10 μm range where high-power lasers are scarce.

A picosecond CO_2 laser is a good candidate for a mid-IR SC generator. For this purpose, GaAs is a particularly attractive material because it has a large nonlinear index of refraction [10], exhibits negative GVD for wavelengths longer than 6.6 μm, and is commercially available in large sizes. The large nonlinear index, approximately 1000 times that of fused silica, may allow for SC generation in a relatively short interaction length while the dispersion of GaAs should facilitate significant spectral broadening at CO_2 laser wavelengths.

To date there is only one reported experiment where a SC spectrum from 3 to 14 μm was generated in GaAs pumped by intense CO_2 laser pulses [11]. In this experiment, 600 μJ, 2.5 ps laser pulses with a central wavelength of 9.3 μm were focused to an intensity of 10^{11} W/cm^2 in a GaAs crystal. Due to these pulse parameters, the researchers observed spectral broadening dominated by SPM.

In this Letter, we report on the generation of mid-IR SC radiation in a 67 mm long GaAs crystal pumped by 3 ps, 2 GW, CO_2 laser pulses with a central wavelength of 10.6 μm. In the experiment, the laser beam propagates through the crystal at an intensity of $\sim 10^{10}$ W/cm^2. We pump the GaAs crystal with a train of 3 ps pulses acting over approximately 100 ps, the duration of a modulated macropulse naturally produced in a CO_2 gain medium [12]. We observe a SC spectrum that features strong Raman components and spans over 135 THz, from 2 to 20 μm. To the best of our knowledge, this is the largest spectral broadening achieved in mid-IR via nonlinear optical techniques.

Figure 1(a) depicts the experimental setup for spectral and temporal characterization of the SC radiation. Semi-insulating GaAs crystals with a length of 2, 30, 67, and 2×67 mm were used in the experiment. The 20 mJ laser pulse train was focused to a peak intensity of $\sim 10^{10}$ W/cm^2 (spot size 2 mm) in order to remain below the damage threshold of the crystal. After the beam exits the GaAs crystal, it is split into two arms. One arm, as shown in Fig. 1, is used to measure the SC spectrum with a monochromator in combination with a liquid N_2 cooled HgCdTe detector. The second arm is used to measure the temporal structure of the output radiation with a streak camera.

The CO_2 laser system, capable of producing 20 GW, 10 μm pulses at a repetition rate of 1 Hz, is described elsewhere [12]. Due to amplification of a short pulse in the CO_2 medium, the temporal structure of the laser pulse is a series of 3 ps pulses, which are separated by 18.5 ps, a time constant related to a residual 55 GHz modulation in the gain spectrum of the CO_2 molecule. Figure 1(b) shows the temporal profile of the picosecond CO_2 pulse train as measured by a streak camera.

Since the temporal measurements are performed using a streak camera, the 10 μm radiation is first converted to visible light by copropagating the output radiation with a red diode probe laser through a CS_2 Kerr cell [13]. Due to the fast (~1 ps) response time of CS_2, this interaction effectively transcribes the temporal information of the 10 μm pump to the visible probe. It should be noted that, due to the finite response time of CS_2, the temporal

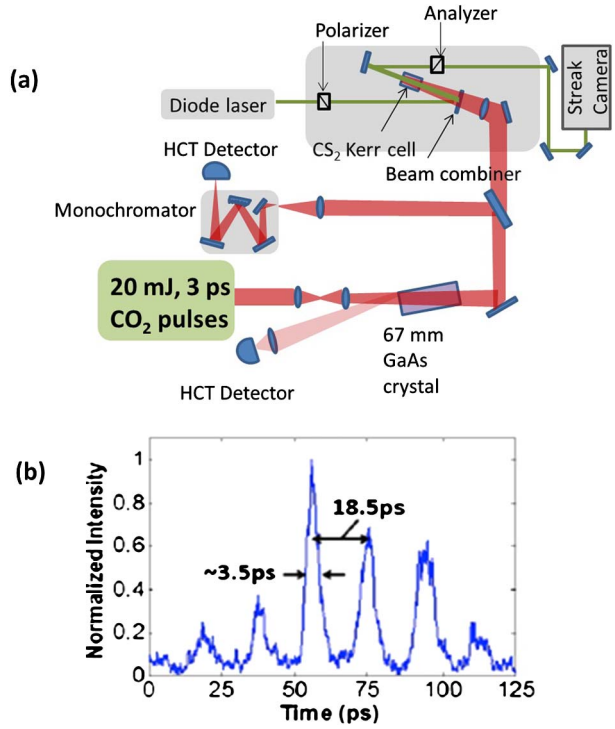

Fig. 1. (a) Simplified experimental setup. HCT is a HgCdTe detector. (b) Typical picosecond 10 μm pulse train used for SC generation.

measurements presented here correspond only to frequency components near the carrier.

In order to experimentally study the evolution of the output spectrum as a function of crystal length, we first used 2 and 30 mm long GaAs crystals. The 2 mm long crystal did not produce significant spectral broadening. Figure 2 shows the measured SC spectrum after the picosecond 10 μm pulse train has propagated through 30 mm of GaAs. Each data point represents an average over three shots of comparable input energy. The latter was measured by reflecting <1% from the AR coated input face of the crystal. We have corrected the data for the spectral response of the monochromator and detector used for the measurement.

The spectrum depicted in Fig. 2 has a bandwidth of 135 THz, from 2 to 20 μm, and is limited by the transmission of the material [14]. The spectrum contains a feature

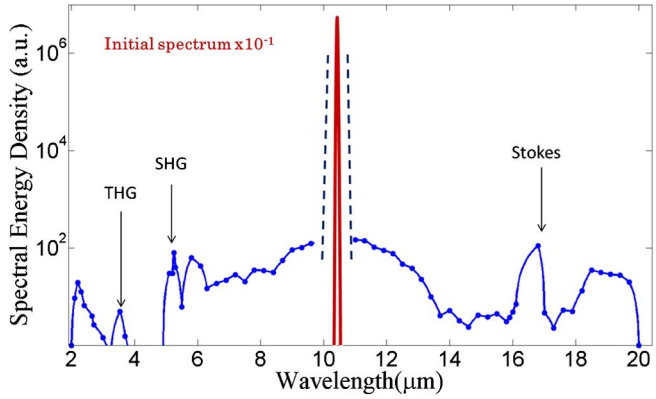

Fig. 2. Experimentally measured spectrum generated in a 30 mm GaAs crystal. SHG and THG stand for second- and third-harmonic generation, respectively.

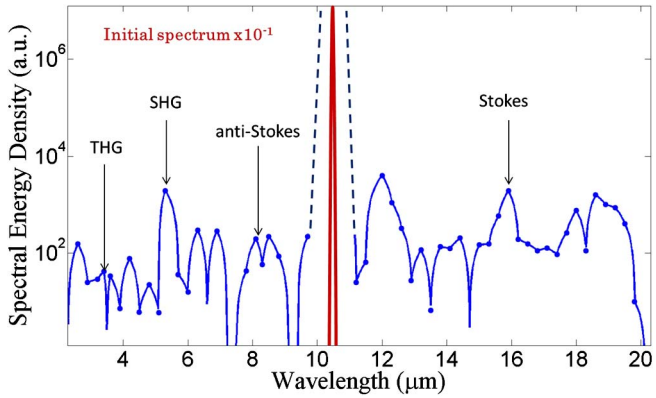

Fig. 3. Experimentally measured spectrum generated in a 67 mm long GaAs crystal. SHG and THG stand for second-harmonic and third-harmonic generation, respectively.

related to the 8.55 THz Raman shift in GaAs [15], which results in a Stokes peak near 16 μm. Harmonic generation results in features at 5.3 and 3.5 μm.

Figure 3 depicts the SC spectrum generated in 67 mm of GaAs. In this case, a long wavelength plateau from 11 to 20 μm with an order of magnitude greater yield than in Fig. 2 was observed. We also observe anti-Stokes and Stokes peaks at 8 and 16 μm, respectively. In contrast to the SC spectrum generated in 30 mm of GaAs, the spectrum after 67 mm of propagation is more modulated. This structure in the SC spectrum is suggestive of temporal breakup of the pump pulse. The existence of the latter was confirmed by time-resolved measurements of the laser pulse after the crystal.

Figure 4 summarizes measurements of the temporal structure of the pulse train, before and after the 67 mm long crystal. As can be seen in Fig. 4(b), although the output pulses retain their initial 18.5 ps modulation, there

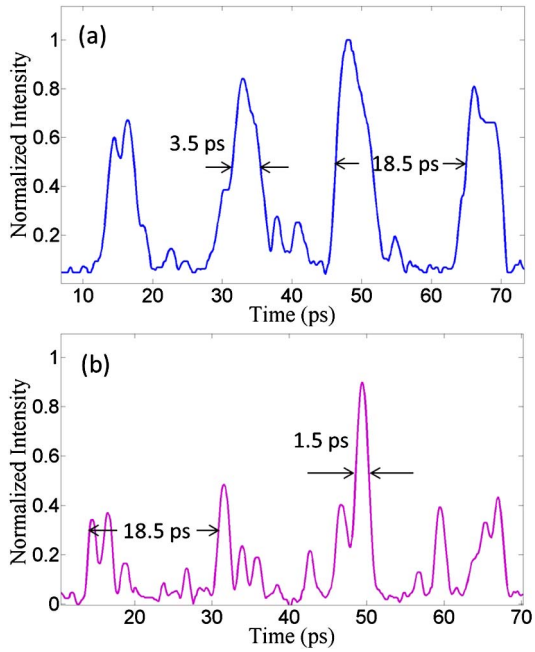

Fig. 4. (a) Input pulse profile zoomed in the vicinity of maximum peak power. (b) Temporal pulse profile after propagating through 67 mm of GaAs.

is an additional, faster modulation, which splits the main pulses into a series of subpulses.

The subpulses presented in Fig. 4(b) are measured to be 1.5 ps, which is limited by the temporal resolution of the streak camera. However, the results of numerical simulations, discussed below, suggest that these pulses can be as short as hundreds of femtoseconds. It should be noted that pulse breakup was not observed after propagation through the 2 or 30 mm long crystal.

In general, the observed pulse splitting can result from MI, SF, or a combination of these phenomena [16]. According to the numerical studies presented in [9], nonlinear optical interactions with a soliton order N larger than ~16 tend to be dominated by MI while interactions with a soliton order less than ~16 tend to be dominated by SF. For our laser pulse parameters and the GaAs GVD coefficient $\beta_2 \approx -1.34(\mathrm{ps}^2/\mathrm{m})$, we calculate a soliton order $N = \sqrt{(L_D/L_{\mathrm{NL}})} \approx 45$. With this soliton order, the observed temporal pulse breakup may be attributed to MI. Additional measurements of the spectral coherence of the SC radiation are necessary to determine whether MI or SF plays a more dominant role in SC generation in 10 μm pumped GaAs [9].

In addition to the results described above, we have studied SC generation in 134 mm of GaAs by using two 67 mm crystals in tandem. Although the energy throughput was nearly 100%, we did not observe a significant increase in the output on the long-wavelength side of the spectrum.

We evaluated the conversion efficiency by sending the undispersed SC radiation through a narrow bandpass filter centered at 12.1 μm and found that, for the 67 mm long crystal, the yield on the long-wavelength plateau is approximately 10^{-5} relative to the carrier (see Fig. 3). This conversion efficiency corresponds to a spectral energy density of 200 $\mathrm{pJ\,nm^{-1}}$–2 $\mathrm{nJ\,nm^{-1}}$, which is comparable with spectral energy densities of supercontinua-generated via laser filamentation [17].

We have modeled the propagation of picosecond CO_2 laser pulse trains through GaAs by numerically solving the generalized nonlinear Schrödinger equation [18]. In doing so, we have used a train of 3 ps pulses similar to that observed in experiment as an input pulse. We have used the dispersion $\beta(\omega)$ of GaAs measured by Skauli *et al.* [19] and have included up to the eighth term in the Taylor series approximation of $\beta(\omega)$. Even though second-order nonlinear processes should play an important role in SC generation in GaAs, simulations were limited to third-order processes responsible for SPM and Raman scattering, signatures of which are apparent in Fig. 2. The Raman response was modeled as an exponentially decaying sinusoid with a frequency of 8.55 THz and a bandwidth of 1 THz, as measured by Ardilla *et al.*. [15]. We have included up to the first derivative of the nonlinear response and have used a Kerr index of $n_2 = 1.7 \times 10^{-4}$ $\mathrm{cm^2/GW}$ for GaAs [10]. In order to match the SC yield observed in experiment, we needed to simulate a pulse train with 35% of the peak power as was measured. We attribute this difference to the fact that we modeled a 1D plane wave as opposed to a real Gaussian beam. Finally, a stochastic amount of noise with a standard deviation equal to the square root of the photon number in one temporal discretization bin was included on the input pulse profile as prescribed in [9].

Figures 5(a) and 5(b) depict the simulated spectrum and temporal pulse profile after the picosecond CO_2 pulse train propagates through 67 mm of GaAs. The spectrum has a bandwidth of approximately 45 THz, from 5 to 20 μm, and contains features that are similar to those observed in experiments. Figure 4(b) shows that spectral broadening is accompanied by the splitting of the most intense pulses in the train into a series of 0.1–0.3 ps subpulses.

To gain insight in the contribution of Raman scattering to SC generation in GaAs, we have performed the same simulation but with SRS disabled. The resulting spectrum and temporal pulse profile are shown in Figs. 4(c) and 4(d), respectively. Comparison of Figs. 4(a) and 4(c) shows that SRS acts to fill in the section of the spectrum in the vicinity of 16 μm. In addition, although Fig. 4(d) shows significant pulse breakup, this effect is not as profound as in the case with SRS enabled [Fig. 4(b)].

Finally, in order to understand the effect of MI on SC generation in 10 μm pumped GaAs, we performed the same simulation discussed above without temporal noise. Figures 5(e) and 5(f) depict the resulting spectrum and temporal pulse profile. Similar to disabling SRS, removing the input noise from the pulse profile delays the onset of pulse breakup and results in significant reduction in the yield on the long-wavelength plateau.

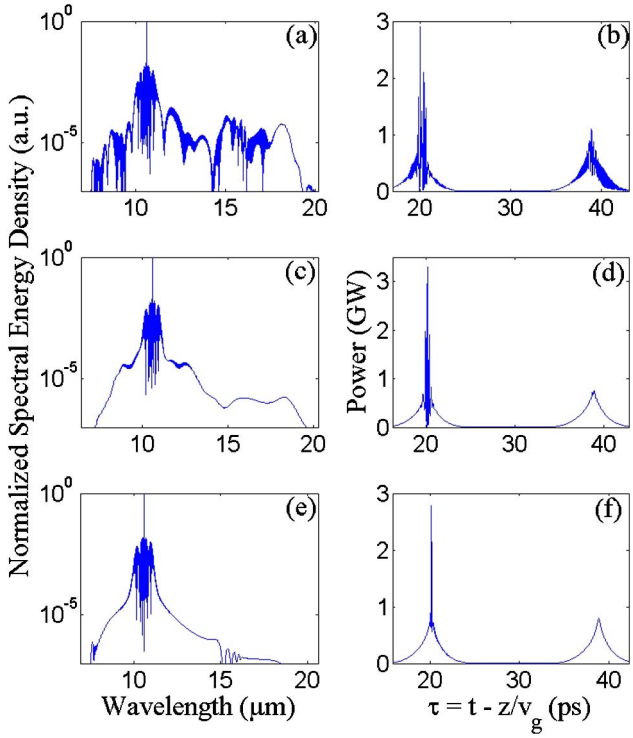

Fig. 5. (a), (c), and (e) Simulated SC spectra and (b), (d), and (f) temporal pulse profile in the vicinity of the two most intense pulses after propagating through 67 mm of GaAs. (c) and (d) Represent results obtained with SRS disabled. (e) and (f) Represent results obtained without noise. Note: while we have simulated a full picosecond CO_2 pulse train, (b), (d), and (e) are zoomed on the two most intense pulses in the train.

In general, several observables in the simulations are in good agreement with those in the experiment. For example, the simulation predicts well the qualitative shape of the SC spectrum and pulse splitting in the time domain. Further, the relative yield between SRS and the frequency components on the long-wavelength plateau agree well with our experimental measurements (Fig. 3).

The main discrepancies between the experimental and simulated spectra are on the high-frequency side of the spectrum. Since we have not included the effect of third-and fifth-harmonic generation in the model, it is not surprising that we were unable to reproduce these features. Another significant limitation of the model is the fact that we do not consider second-order (i.e., $\chi^{(2)}$) processes. From the observed second-harmonic yield, it is clear that second-order processes play an important role in SC generation in GaAs. For example, difference frequency generation between various spectral components may contribute to the observed structure in the SC spectrum. Higher-resolution spectral measurements are needed to determine if the structure seen on both the high- and low-frequency side of the spectrum is attributable to wave–wave mixing processes.

We also modeled spectral broadening in GaAs pumped by CO_2 laser wavelengths shorter than 10.6 μm, specifically 9.3 μm (9-R-branch). This has revealed that a shift toward the zero-dispersion wavelength causes spectral broadening dominated by SPM, which is similar to that recorded by Corkum *et al.* [11]. Linear frequency chirping via SPM followed by compression using dispersive optical elements in this regime may open an avenue to obtain sub-picosecond mid-IR pulses.

In summary, we have generated a SC spectrum from 2 to 20 μm by propagating a picosecond CO_2 pulse train through a 67 mm long GaAs crystal. Based on experimental observations, it appears that the dominant mechanisms for SC generation in 10 μm pumped GaAs are FWM and SRS. The SC is limited by the bandgap on the blue side and the phonon band on the red side of the spectrum. Usage of different materials (e.g., CdTe) may extend the SC spectrum even further to ~30 μm.

It should be mentioned that the CO_2 laser pump can be scaled in a repetition rate to hundreds of Hz thus opening the possibility to build SC-based sources for different applications.

We would like to thank our anonymous reviewers for their helpful comments and suggestions. This study was supported by U.S. Department of Energy grant DE-SC0010064.

References

1. R. R. Alfano, *The Supercontinuum Laser Source* (Springer, 2006).
2. J. W. Nicholson, M. F. Yan, P. Wisk, J. Fleming, F. DiMarcello, E. Monberg, and A. Yablon, Opt. Lett. **28**, 643 (2003).
3. B. R. Washburn, S. A. Diddams, N. R. Newbury, J. W. Nicholson, M. F. Yan, and C. G. Jørgensen, Opt. Lett. **29**, 250 (2004).
4. A. Marandi, C. W. Rudy, V. G. Plotnichenko, E. M. Dianov, K. L. Vodopyanov, and R. L. Byer, Opt. Express **20**, 24218 (2012).
5. C. W. Rudy, A. Marandi, K. L. Vodopyanov, and R. L. Byer, Opt. Lett. **38**, 2865 (2013).
6. F. Théberge, J. Daigle, D. Vincent, P. Mathieu, J. Fortin, B. E. Schmidt, N. Thiré, and F. Légaré, Opt. Lett. **38**, 4683 (2013).
7. S. Coen, H. L. Chau, R. Leonhardt, J. D. Harvey, J. C. Knight, W. J. Wadsworth, and P. St. J. Russell, Opt. Lett. **26**, 1356 (2001).
8. C. Xia, M. Kumar, O. P. Kulkarni, M. N. Islam, F. L. Terry, Jr., M. J. Freeman, M. Poulain, and G. Mazé, Opt. Lett. **31**, 2553 (2006).
9. J. M. Dudley, G. Genty, and S. Coen, Rev. Mod. Phys. **78**, 1135 (2006).
10. C. A. Kapetanakos, B. Hafizi, H. M. Milchberg, P. Sprangle, R. F. Hubbard, and A. Ting, IEEE J. Quantum Electron. **35**, 565 (1999).
11. P. B. Corkum, P. P. Ho, R. R. Alfano, and J. T. Manassah, Opt. Lett. **10**, 624 (1985).
12. S. Ya. Tochitsky, J. J. Pigeon, D. J. Haberberger, C. Gong, and C. Joshi, Opt. Express **20**, 13762 (2012).
13. C. V. Filip, R. Narang, S. Ya. Tochitsky, C. E. Clayton, and C. Joshi, Appl. Opt. **41**, 3743 (2002).
14. C. J. Johnson, G. H. Sherman, and R. Weil, Appl. Opt. **8**, 1667 (1969).
15. A. M. Ardilla, O. Martínez, M. Avella, J. Jiménez, B. Gérard, J. Napierala, and E. Gil-Lafon, J. Appl. Phys. **91**, 5045 (2002).
16. A. Demircan and U. Bandelow, Appl. Phys. B **86**, 31 (2006).
17. F. Silva, D. R. Austin, A. Thai, M. Baudisch, M. Hemmer, D. Faccio, A. Couairon, and J. Biegert, Nat. Commun. **3**, 807 (2012).
18. G. P. Agarwal, *Nonlinear Fiber Optics* (Academic, 2001).
19. T. Skauli, P. S. Kuo, K. L. Vodopyanov, T. J. Pinguet, O. Levi, L. A. Eyres, J. S. Harris, and M. M. Fejer, J. Appl. Phys. **94**, 6447 (2003).